Eigenstate thermalization scaling in approaching the classical limit

Goran Nakerst [1] and Masudul Haque [1,2]
[1]*Department of Theoretical Physics, Maynooth University, Co. Kildare, Ireland*
[2]*Max-Planck-Institut für Physik komplexer Systeme, D-01187 Dresden, Germany*

(Received 5 January 2021; accepted 16 March 2021; published 5 April 2021)

According to the eigenstate thermalization hypothesis (ETH), the eigenstate-to-eigenstate fluctuations of expectation values of local observables should decrease with increasing system size. In approaching the thermodynamic limit—the number of sites and the particle number increasing at the same rate—the fluctuations should scale as $\sim D^{-1/2}$ with the Hilbert space dimension D. Here, we study a different limit—the classical or semiclassical limit—by increasing the particle number in fixed lattice topologies. We focus on the paradigmatic Bose-Hubbard system, which is quantum-chaotic for large lattices and shows mixed behavior for small lattices. We derive expressions for the expected scaling, assuming ideal eigenstates having Gaussian-distributed random components. We show numerically that, for larger lattices, ETH scaling of physical midspectrum eigenstates follows the ideal (Gaussian) expectation, but for smaller lattices, the scaling occurs via a different exponent. We examine several plausible mechanisms for this anomalous scaling.

DOI: 10.1103/PhysRevE.103.042109

I. INTRODUCTION

During the past decade and a half, a considerable amount of research has focused on understanding how isolated quantum systems can relax and thermalize. A cornerstone of this understanding is the Eigenstate thermalization hypothesis (ETH) [1–9]. According to the ETH, the diagonal matrix elements of observables in the eigenstate basis of the Hamiltonian, the eigenstate expectation values (EEV), coincide locally with the microcanonical ensemble. This means that the EEVs vary smoothly as a function of energy eigenvalues. The smoothness is quantified as the fluctuations of the EEVs being exponentially small as a function of the system size.

A standard quantitative statement of ETH states that the matrix elements of an operator A representing a typical physical observable should have the form [3,4]

$$\langle E_\alpha|A|E_\beta\rangle = \delta_{\alpha\beta} f_A^{(1)}(\bar{E}) + e^{-S(\bar{E})/2} f_A^{(2)}(\bar{E},\omega) R_{\alpha\beta}, \qquad (1)$$

where S is the entropy, $|E_\alpha\rangle$ is an energy eigenstate with eigenenergy E_α, $\bar{E} = (E_\alpha + E_\beta)/2$, and $\omega = E_\beta - E_\alpha$. The $f_A^{(1/2)}$ are smooth functions, and $R_{\alpha\beta}$ is a (pseudo)random variable with zero mean and unit variance. For systems with finite Hilbert space dimension D, the entropy scales as $S \sim \log D$. Thus, a crucial aspect of ETH is the scaling of the width of the distribution of either diagonal or off-diagonal matrix elements: When approaching the thermodynamic limit, this width falls off as $e^{-S/2} \sim D^{-1/2}$, i.e., exponentially with system size. This scaling can be understood using the similarity between typical many-body eigenstates and random states [10–12]. This behavior contrasts sharply with integrable systems, which do not obey ETH scaling—the width of diagonal matrix element distributions generally have power law decay with system size [11,13–19], and the off-diagonal matrix element generally has a non-Gaussian distribution [12,18,20].

Evidence from a large number of numerical studies strongly suggests that ETH is satisfied for eigenstates from the bulk of the spectrum of generic nonintegrable systems and for physical observables [5,9–12,18,19,21–46]. In particular, several studies have examined the decrease of the width of matrix element distributions as the thermodynamic limit is approached, both for chaotic and integrable systems [11–19,28,31,36,40,43–45,47–49]. For lattice systems, the thermodynamic limit involves increasing both the lattice size and the particle number simultaneously, keeping the average density fixed. In the present work, we will instead explore approaching the *classical limit*—we consider increasing particle numbers in fixed lattice topologies. We investigate the scaling behavior of EEV fluctuations as a function of Hilbert space dimension, as the classical limit is approached.

We focus on Bosonic systems and study the Bose-Hubbard Hamiltonian on fixed numbers of sites. The dynamics of these systems in the classical limit have been extensively studied, where they are described by a discrete nonlinear Schröedinger equation. Because of the existence of a classical limit, Bose-Hubbard systems have also been extensively used as a testbed for semiclassical methods [50–69]. Quantum dynamics of these systems have also been compared with the dynamics of the corresponding classical limit [70–76].

We consider N particles in k sites, arranged linearly. We approach the large limit of large Hilbert space dimension ($D \to \infty$) by keeping k fixed and increasing N, as opposed to the usual thermodynamic limit for which the ratio N/k would be kept fixed. The two-site system (Bose-Hubbard dimer, $k = 2$) is integrable, and hence we omit this case in the present work on ETH scaling. We focus on lattices with sizes from $k = 3$ up to $k = 10$. The case of $k = 3$ (and to a lesser extent $k = 4$) is particularly interesting: although not integrable, the classical phase space in this case is known

to be highly "mixed" [53,72,76–81], and the behavior of the finite-N quantum system shows deviations from fully chaotic behavior. For larger site numbers, $k \gtrsim 5$, the Bose-Hubbard systems tend to behave as quantum-chaotic systems [74,82–85].

Assuming the eigenstates to be perfectly ergodic "infinite-temperature" states in the sense of having Gaussian-distributed random coefficients, an exact formula for the EEV fluctuations is available. This relation [Eq. (7)] only depends on trace expressions of operators, and holds for all operators, as long as the "Gaussian eigenstates" approximation is valid. It mathematically connects the Gaussianity of eigenstates to finite size scaling of ETH, and provides an alternate derivation of ETH scaling.

The class of observables generally considered in ETH investigations (observables of physical interest) are few-body operators or sums thereof, i.e., "local" operators. However, having k fixed and small means that the notion of "local" operators has to be re-examined. When considering $k \to \infty$, two-site operators are local in the sense that $2 \ll k$. This is no longer true for our constant k; in particular it is strongly violated for $k = 3$. Therefore, we re-examine the expected scaling of EEV fluctuations, first for Gaussian eigenstates. We show that the expected behavior for $N \gg k$ is $\sim D^{-e_0}$ with $e_0 = \frac{1}{2} - \frac{1}{k-1}$. The exponent ranges from $e_0 = 0$ for the three-site case ($k = 3$) to $e_0 \to \frac{1}{2}$ for large k ($N \gg k \gg 1$).

The scaling exponent e_0 being different from $1/2$ for moderate k can be traced to the unboundedness of the operators in the $N \to \infty$ limit. The $D^{-1/2}$ scaling could be retrieved by renormalizing the operators A and considering operators $\bar{A} = A/N$.

For the actual midspectrum eigenstates of the Bose-Hubbard chains, we show numerically that the EEV fluctuations match the behavior predicted by the Gaussian ansatz, once k is large enough. For small k, the dependence on D is seen to be a power law but with a *different* exponent $e \neq e_0$. This is a remarkable manifestation of the "mixed" nature of the three-site and four-site Bose-Hubbard systems.

At present, we do not have a predictive explanation for the observed exponents. Small or subleading deviations from Gaussian behavior (from random-matrix behavior) has been noted previously in midspectrum eigenstates of chaotic many-body systems. Such deviations can be seen in the eigenstate coefficient distribution in the configuration basis [37,86–88], in the entanglement entropy of eigenstates [20,89–91], and in the fluctuations of off-diagonal matrix elements [45]. Since the present $k = 3$ system has strong nonchaotic features, it is not surprising that there is even stronger deviation from Gaussian-state behavior. Perhaps unexpectedly, EEV fluctuations show a clear power law dependence on the Hilbert space dimension, but the exponent is markedly different from the random-matrix prediction. This demonstrates that eigenstates of small-k Bose-Hubbard chains have nonrandom correlations. We examine the most straightforward ways in which physical eigenstates could be different from ideally ergodic eigenstates, e.g., non-Gaussian coefficient distributions and two-point correlations between the eigenstate coefficients. We demonstrate that none of these effects explain our observed scaling. The observed scaling exponent thus results from more subtle structures in the eigenstate coefficients, which seems challenging to characterize or identify.

In Sec. II we introduce the system, notations, and the numerical procedure for extracting EEV fluctuations σ. Section III is the heart of the paper and reports the main results: analytically derived trace expressions and scaling laws for σ in the case of idealized (Gaussian) eigenstates (Sec. III A), and results of extensive numerics showing where these predictions succeed and where they fail (Sec. III B). In Sec. IV we examine possible reasons for the few site systems (particularly $k = 3$) deviating from the Gaussian prediction and displaying anomalous exponents in the D-dependence of σ. We conclude that the anomalous scaling is due to subtle higher-order correlations among the eigenfunction coefficients which cannot be captured by the two-point correlations among eigenfunction components. Sec. V provides context and concluding discussion.

The Appendices present further details, data and clarification. We show the dependence on the interaction parameter and justify the interaction value used in the main text (Appendices A and B). We display the structure of covariance matrices of the physical eigenstates (C). Appendices D and E contain the derivations of the analytic results announced in the main text.

II. PRELIMINARIES—SYSTEMS AND OBSERVABLES

In this section, we introduce the system Hamiltonian (Sec. II A), discuss how to define the fluctuations of the EEVs (Sec. II B), and introduce notation to be used in this paper.

A. Hamiltonians

We will investigate Bose-Hubbard systems restricted to open-boundary chains of length k, with nearest-neighbor hoppings and onsite interactions. The Hamiltonian is

$$H = -1/2 \sum_{\langle i,j \rangle} J_{i,j} a_i^\dagger a_j + \frac{U}{2} \sum_{j=1}^{k} n_j (n_j - 1), \tag{2}$$

where $\langle i, j \rangle$ denotes summation over adjacent sites ($j = i \pm 1$), $a_j^\dagger$ and a_j are the Bosonic creation and annihilation operators for the jth site and $n_j = a_j^\dagger a_j$ is the corresponding occupation number operator. $J_{i,j} = J_{j,i}$ is the symmetric tunneling coefficient and U is the two-particle onsite interaction strength. We choose $J_{1,2} = 1.5$ and $J_{i,j} = 1$ for $i, j \geqslant 2$ to avoid reflection symmetry. The particle number N is conserved by the Hamiltonian. We introduce the tuning parameter $\Lambda = UN$.

In the limits $\Lambda \to 0$ and $\Lambda \to \infty$ the system is integrable. If $\Lambda = 0$, then the free Bosonic system is solvable in terms of single-particle eigenstates, while $\Lambda \to \infty$ effectively means J can be neglected, so that Eq. (2) is diagonal already. For intermediate Λ the systems behave chaotically, i.e., the spectrum approximately obeys Wigner-Dyson statistics. For the smallest chain length $k = 3$, there are stronger deviations, but nevertheless the spectral statistics near the middle of the spectrum is close to Wigner-Dyson form (Appendix A).

The Hilbert space size is $D = \binom{N+k-1}{k-1} = \binom{N+k-1}{N}$, which scales for fixed k in the large N limit as $D \sim N^{k-1}$.

Therefore, for fixed k in the large D limit, N scales as $N \sim D^{1/(k-1)}$.

The operators we focus on are the tunnel operator $a_2^\dagger a_1$ from site 1 to site 2 and the number operator n_1 on site 1. We have checked that the overall scaling behaviors are the same for $a_i^\dagger a_j$ with other i, j. Note that $a_2^\dagger a_1$ is non-Hermitian. If hermiticity is required, we will instead investigate $(a_2^\dagger a_1 + a_1^\dagger a_2)$. This change results in an additional factor of 2 in the corresponding EEV fluctuation.

B. Defining EEV fluctuations

We denote by $|E_\alpha\rangle$ the eigenstate of the Hamiltonian H belonging to the eigenvalue E_α. If the ETH holds, $A_{\alpha\alpha} = \langle E_\alpha|A|E_\alpha\rangle$ is constant on small energy windows $[E_\alpha - \delta, E_\alpha + \delta]$ around E_α for suitable (small) δ, up to finite size fluctuations. Further, $A_{\alpha\alpha}$ coincides with the microcanonical average

$$\langle A\rangle_{(E_\alpha,\delta)} = \frac{1}{N_{E_\alpha,\delta E_\alpha}} \sum_{\beta:E_\beta\in[E_\alpha-\delta,E_\alpha+\delta]} A_{\beta\beta}. \tag{3}$$

A quantitative measure of how well the EEVs coincide with the microcanonical average is the magnitude of the finite size fluctuations, i.e., the statistical standard deviation of $A_{\alpha\alpha} - \langle A\rangle_{(E_\alpha,\delta)}$,

$$\left[\frac{1}{N_{\Delta E}} \sum_{E_\alpha \text{ in } \Delta E} (A_{\alpha\alpha} - \langle A\rangle_{(E_\alpha,\delta)})^2\right]^{1/2}, \tag{4}$$

over some energy window ΔE, where $N_{\Delta E}$ is the number of eigenvalues E_α in ΔE. Graphically this measures the width of the distribution of $A_{\alpha\alpha}$ values.

The above definition involves a choice of the window width δ; this choice may depend on various parameters of the physical model. To avoid larger scale changes of $A_{\alpha\alpha}$ (e.g., as visible in Fig. 1), the window should not be too wide. The window should also not be too small, so as to ensure that sufficiently many EEVs are within the window around E_α to get a statistically significant estimate of the fluctuations. Choosing δ can thus be a tricky balancing act.

We can avoid these technicalities by noting that ETH implies that the quantity $A_{\alpha\alpha}$ will vary smoothly as a function of E_α, up to finite size fluctuations. If the ETH holds in this sense, then, by definition of smoothness, $A_{\alpha\alpha}$ should be locally linear. We divide the energy spectrum into 10 equal-length, disjoint intervals ΔE. In these intervals the large scale change of $A_{\alpha\alpha}$ in our case is indeed linear to an excellent approximation, as seen in the lower panels of Fig. 1. We fit linear functions $E_\alpha \to b + mE_\alpha$, on each interval to $A_{\alpha\alpha}$. We then investigate the fluctuations around these functions, i.e.,

$$\sigma^2(A, \Delta E) = \frac{1}{N_{\Delta E}} \sum_{E_\alpha \text{ in } \Delta E} |A_{\alpha\alpha} - b - mE_\alpha|^2. \tag{5}$$

Since we are primarily interested in midspectrum eigenstates, we will show data from the 5th, 6th and 7th energy intervals. In shorthand these will be labeled as $\Delta E = 5$, $\Delta E = 6$, $\Delta E = 7$, with ΔE referring to the label and not the interval width. In Fig. 1, we display the EEV's for the full spectrum and for the $\Delta E = 5$ interval, for two different values of k. Unless indicated otherwise, we present data for an intermediate value of the interaction parameter $\Lambda = UN$ around which the systems are found to be significantly chaotic, namely, $\Lambda = 10^{13/33} \approx 2.477$. Appendix A provides further details on this choice of Λ.

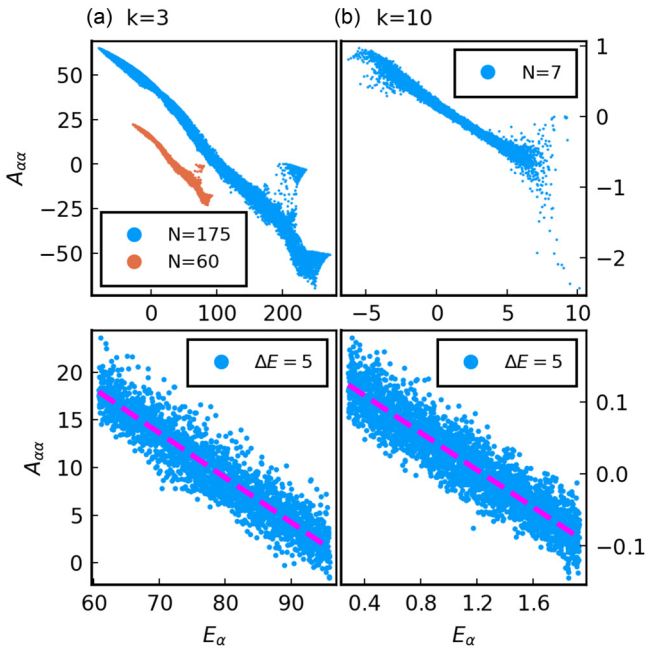

FIG. 1. Eigenstate expectation values $A_{\alpha\alpha}$ of the tunnel operator $A = a_2^\dagger a_1$, plotted against eigenenergies, for a Bose-Hubbard chain with (a) $k = 3$ sites and (b) $k = 10$ sites. The numbers of particles N are listed in legends. In panel (a) the larger cluster corresponds to $N = 175$ particles, while the smaller cluster on the left corresponds to $N = 60$ particles. The interaction parameter is $\Lambda \approx 2.477$ as explained in the text. Top panels show full spectra. Bottom panels zoom into the 5th of ten equal energy intervals, as indicated by the shorthand label "$\Delta E = 5$." Dotted lines are fitted linear functions.

III. EEV FLUCTUATION SCALING

In this section we first (Sec. III A) consider Gaussian-random states, e.g., eigenstates of matrices drawn from the GOE ensemble. We present expressions for the EEV fluctuations for such idealized eigenstates. For operators of the type $A = a_i^\dagger a_j$, we show that the scaling of EEV fluctuations, $\sigma \sim D^{-e_0}$, occurs with exponent $e_0 = \frac{1}{2} - \frac{1}{k-1}$ in the classical limit ($N \to \infty$, fixed k). For normalized operators $\bar{A} = A/N$, the exponent is $e_0 = \frac{1}{2}$. In comparison, in the usual thermodynamic limit ($N \to \infty$, fixed k/N), the exponent is $e_0 = \frac{1}{2}$ for local operators.

Next (Sec. III B), we present numerically calculated scaling results for Bose-Hubbard chains. We show that the EEV fluctuations have power-law dependence on the Hilbert-space dimension, $\sim D^{-e}$. The exponent e matches the Gaussian-state prediction e_0 for larger chains, but differs substantially for small k.

A. Derivation for random Gaussian states

The EEV's calculated for random states do not have large-scale smooth variation as a function of energy, in contrast to Fig. 1. Thus, the statistical standard deviation of EEV's, σ, can be directly compared with our measurement of EEV fluctuations in the physical eigenstates. The assumption of eigenstates being effectively random has been previously used to derive scaling properties of EEV's in the thermodynamic limit [10,11,45]. Here, we provide explicit expressions for σ in terms of trace properties of the operator matrix, and then specialize to both thermodynamic and classical limits. We present the important expressions here, and relegate derivation details to Appendices D and E.

1. Trace expressions

Let A be a $D \times D$ square matrix representing the operator of interest, and $|Z\rangle$ be a D-dimensional, multivariate random state with identically and independently distributed (i.i.d.) components Z_i, each with mean 0. Then the statistical variance of $\langle A\rangle = \langle Z|A|Z\rangle$ can be expressed as

$$\sigma^2(\langle A\rangle) = \left(E\left[Z_1^4\right] - 3E\left[Z_1^2\right]^2\right)\sum_i A_{ii}^2 + E\left[Z_1^2\right]^2[\mathrm{tr}(A^2) + \mathrm{tr}(AA^\dagger)]. \tag{6}$$

Here $E[\cdot]$ represents the expectation value. The manipulations leading to this expression can be found in Appendix D.

Equation (6) is valid irrespective of the distribution of the i.i.d. variables Z_i. Simplifications are achieved by specializing to the case of GOE eigenstates, widely considered as reasonable models for the behavior of midspectrum eigenstates of chaotic Hamiltonians. Eigenstates of D-dimensional Gaussian matrices are uniformly distributed on the D-dimensional unit sphere. In the large D limit their components can be regarded as independently normally distributed with mean 0 and variance $1/D$. If we take Z_i to be normally distributed with variance $1/D$, in addition to the previous constraints, then the first term in Eq. (6) vanishes. Thus,

$$\sigma^2(\langle A\rangle) = \frac{1}{D^2}[\mathrm{tr}(A^2) + \mathrm{tr}(AA^\dagger)] \tag{7}$$

for random states with Gaussian-distributed coefficients.

The second of the two traces, $\mathrm{tr}(AA^\dagger)$, is the squared Hilbert-Schmidt norm or the Frobenius norm of the operator. For Hermitian A the two trace terms are equal: $\mathrm{tr}(A^2) = \mathrm{tr}(AA^\dagger)$. As $\mathrm{tr}(A^2)$ and $\mathrm{tr}(AA^\dagger)$ are invariant under a basis change, so is the variance Eq. (7). In contrast, Eq. (6) is not basis-invariant, due to the first term. Expressions equivalent or analogous to Eq. (7) have appeared previously in the literature, e.g., in Refs. [92–95].

For observables of the form $A = a_j^\dagger a_i$, the trace expression is shown in Appendix E to be given by

$$\mathrm{tr}(A^2) + \mathrm{tr}(AA^\dagger) = \frac{N(N+k)}{k(k+1)}D \quad i \neq j, \tag{8a}$$

$$\mathrm{tr}(A^2) + \mathrm{tr}(AA^\dagger) = \frac{2N(2N+k-1)}{k(k+1)}D \quad i = j. \tag{8b}$$

In the usual thermodynamic limit, the fraction multiplying D has $O(D^0)$ scaling in either case. Thus, one obtains $\sigma^2 \sim \frac{D}{D^2}$, i.e., the usual $\sigma \sim D^{-1/2}$ scaling for EEV fluctuations in the thermodynamic limit.

2. Scaling in the classical limit

We now consider the classical limit, $k \ll N$. If A is a linear combination of terms like $a_j^\dagger a_i$, then the trace expression scales as

$$\mathrm{tr}(A^2) + \mathrm{tr}(AA^\dagger) \sim N^2 D. \tag{9}$$

Since $N \sim D^{1/(k-1)}$ in the classical limit, the variance scales as

$$\sigma^2(\langle A\rangle) \sim \frac{D \cdot D^{2/(k-1)}}{D^2} = D^{-2e_0}, \tag{10}$$

where

$$e_0 = e_0(k) = \frac{1}{2} - \frac{1}{(k-1)} \tag{11}$$

is the scaling exponent announced previously. For $k \gg 1$, but still $k \ll N$, the second term becomes negligible and we obtain $\sigma \sim D^{-1/2}$ scaling similar to the thermodynamic limit.

For numbers of sites that are not too large, the EEV scaling of two-point operators (of the type $a_j^\dagger a_i$ or their linear combinations) is different for the classical limit compared to the thermodynamic limit. Mathematically, this difference can be attributed to the operators A scaling with N. If we renormalize A to $\bar{A} = A/N$, then the traces (9) scale as D rather than as $N^2 D$, so that the variance scales for all k as

$$\sigma^2(\langle \bar{A}\rangle) \sim \frac{D}{D^2} = D^{-1}. \tag{12}$$

Summarizing: In the classical limit, the EEV fluctuation scaling is $\sim D^{-1/2}$ for normalized operators $\bar{A} = A/N$ for all k and also for unnormalized operators A in the $k \gg 1$ limit. This is the same exponent $e_0 = \frac{1}{2}$ familiar from the thermodynamic limit [11,45]. However, for moderate k and for the operator A, the scaling is according to the exponent $e_0 = \frac{1}{2} - \frac{1}{(k-1)}$ of Eq. (11)

B. Numerical results: Bose-Hubbard eigenstates

In Fig. 2 we show the fluctuations σ of the EEVs for different energy windows near the middle of the spectrum, plotted against D. Each panel shows a different (fixed) number of sites k; in each case the classical limit is approached by increasing N. Generally, the sequences follow clear power-law dependencies, $\sigma \sim D^{-e}$. The power-law behavior sets in at relatively small values of D already.

It is clear from the $k = 3$ data, panel (a), that the exponent e does not match the value predicted for Gaussian-random states, Eq. (11), which is $e_0 = 0$ for $k = 3$. The EEV fluctuation for the system eigenstates *increases* with a positive exponent ($e < 0$) instead of being flat as a function of D. Similarly, for the four-site chain the exponent e is seen to be slightly negative—σ increases slowly with system size—whereas the predicted value is $e_0 = +1/6$.

The calculations rely on full numerical diagonalization, and hence are limited by the Hilbert space size D. Our limit was $D \lesssim 10^5$. For each k, we increased the particle number N as far as possible such that D did not exceed 100 000. For

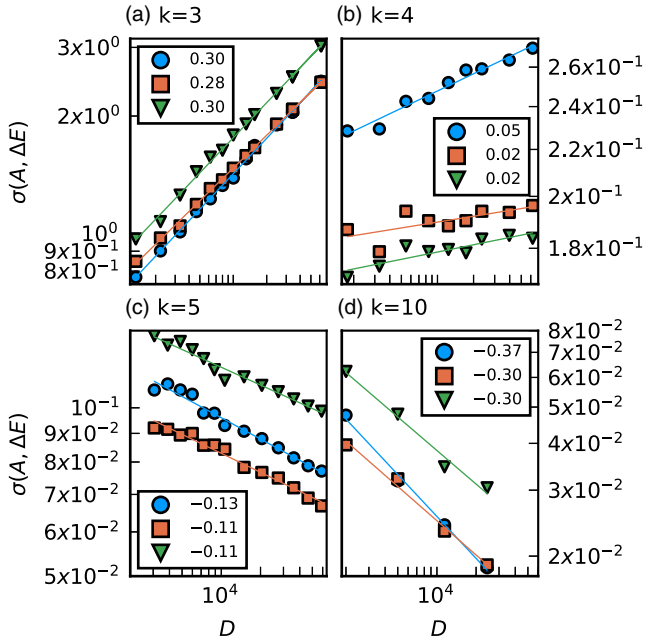

FIG. 2. EEV fluctuations σ of the operator $A = a_2^\dagger a_1$ against Hilbert space size D for various chain lengths k. Data shown for eigenstates in energy windows $\Delta E = 5$ (blue circles), 6 (red squares), 7 (green inverted triangles). The σ vs D data sequences are arranged reasonably linearly in all cases in the log-log plots, suggesting $\sigma \sim D^{-e}$ behavior. The slopes of fitted lines (i.e., numerical estimates of $-e$) are given in the legends. The Gaussian predictions e_0 for the exponents are 0, $\frac{1}{6} \approx 0.1667$, 0.25, and $\frac{7}{18} \approx 0.3889$ respectively for $k = 3$, 4, 5, and 10.

small k, this provides a satisfactory number of available N values, and extracting the exponent e from a fit to $\sigma \sim D^{-e}$ is quite reliable. For large k, only a few N values are available. For the largest lattice ($k = 15$), only three data points ($N = 4$, $N = 5$, and $N = 6$) were used. This means a large uncertainty in the estimation of e (Fig. 3 inset). It also means that the regime $N \gg k$ is not reached.

In Fig. 3 we present the exponents e extracted from the numerical data. In addition to the exponents for the operator $a_2^\dagger a_1$ (corresponding to Fig. 2), we also show the exponents for the operator n_1. For small k, the numerically observed exponents e fall significantly below the Gaussian-random case, for both operators. For larger k values, the Bose-Hubbard systems show EEV fluctuations closer to the Gaussian-random case, at least for $\Delta E = 5, 6$. (The $\Delta E = 7$ window shows larger deviation, presumably becuase it is closer to the edges of the spectrum.) We interpret this as a signature of the large-k Bose-Hubbard systems being more chaotic, so that midspectrum eigenstates are better approximated by Gaussian-random states. The deviation for small k represents the "mixed" (chaotic+regular) nature of the few-site Bose-Hubbard Hamiltonians.

Figure 3 also shows numerically calculated exponents for EEV fluctuations in Gaussian-random states (pink triangles), and compares with the $k \ll N$ prediction, Eq. (11) (pink dashed curve). The agreement is good for all k and excellent for small k. At larger k, computer memory limitations prevent our calculations from reaching particle numbers $N \gg k$. This

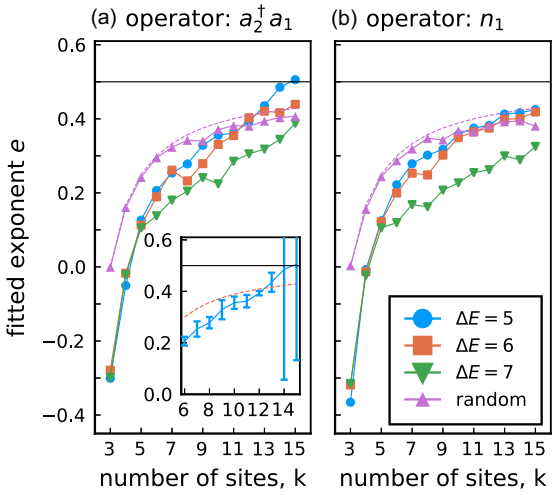

FIG. 3. The exponent e versus the chain length k for Bose-Hubbard eigenstates in different energy windows, and for Gaussian-random states. The pink dashed curve is the predicted formula for exponents, e_0, which tends to 1/2 (solid horizontal line) for large k. Inset to left panel shows the error bars for the estimation of e from $\Delta E = 5$ data. The error bars are omitted elsewhere and will be omitted in later figures.

explains the (minor) deviation of the numerical exponents from the $N \gg k$ prediction.

One can view the same effects through the fluctuations of the normalized ($\bar{A}$) operators $a_2^\dagger a_1/N$ and n_1/N. For these operators, the predicted exponent is 1/2 for all k. We present the numerical exponents for such operators in Fig. 4; however, we normalize by factors slightly different from N. The prediction

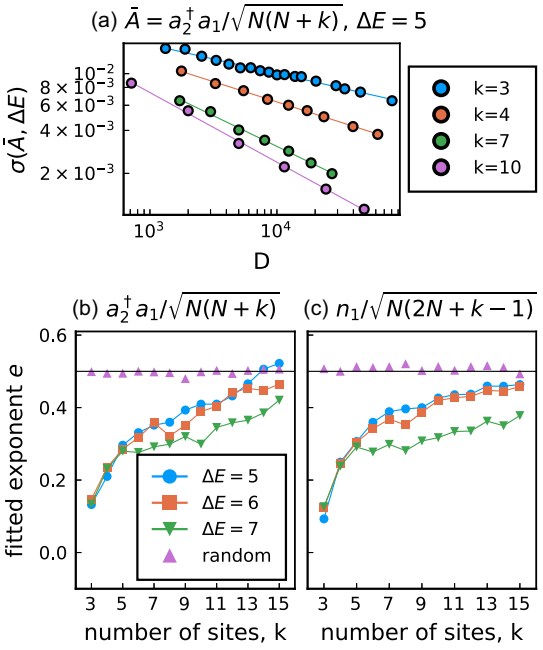

FIG. 4. Similar data as in Figs. 2 and 3 but with normalized operators $\bar{A}$. The operators are normalized by factors $\sim N$; the precise factors are explained in the text. (a) Points and fits are from top to bottom $k = 3$, $k = 4$, $k = 7$, and $k = 10$.

$e_0 = 1/2$ was obtained in the previous subsection by assuming $N \gg k$. In particular in the trace expressions of Eq. (8), this led to $N(N+k) \approx N^2$ and $2N(2N+k-1) \approx 4N^2$. In our numerical calculations, for larger k we do not have access to N values in this regime. Therefore, we normalize the operators by the factor $\sqrt{N(N+k)}$ for $A = a_i^\dagger a_j$ with $i \neq j$ and by the factor $\sqrt{N(2N+k-1)}$ for $i = j$. With this modification, the numerically calculated exponents using Gaussian-random states (pink triangles) do not deviate systematically from $1/2$ at large k, even though the $N \gg k$ regime is not reached. The observed physical exponents (for Bose-Hubbard eigenstates) are significantly different from the predicted $e_0 = 1/2$ for small k, but approach this value as k is increased.

Summarizing our numerical findings: Power-law dependence of EEV fluctuations on D is seen for all k. The exponent at larger k (more fully chaotic systems) matches well the Gaussian prediction. For smaller k (mixed systems), there are significant deviations from the Gaussian prediction. Remarkably, for small k, the departure of the eigenstates from Gaussian-random or ergodic behavior does not destroy the power-law dependence of EEV fluctuations with D but changes the exponent substantially. In fact, for the smallest sizes ($k = 3$ and $k = 4$) the numerically measured exponent e even turns negative for unnormalized operators, so fluctuations of EEVs actually *grow* with N.

In the following section we will examine possible explanations for this phenomenon.

IV. NONREASONS FOR ANOMALOUS SCALING

The mismatch with predicted scaling for small k must be due to the eigenstates of few-site Bose-Hubbard systems deviating from idealized Gaussian-random states, which we refer to as "ergodic" states. In this section, we examine various types of deviation from the idealized case, and rule out several plausible explanations for the anomalous scaling.

One could imagine that the eigenstates effectively occupy a smaller fraction of the Hilbert space than a random state, and that this fraction has sublinear scaling with D. This can be quantified through analysis of the participation ratio or multifractal dimensions of the eigenstates. Therefore, in Sec. IV A, we discuss the participation ratio P_α. We show how $P_\alpha \sim D^1$ scaling implies the expected EEV fluctuation scalings that we have derived previously in Sec. III A. We also show that Hilbert space occupancy is not the explanation for our anomalous EEV scaling exponents, because eigenstates of the $k = 3$ system have $P_\alpha \sim D^1$ scaling.

One could also imagine that the anomaly of scaling exponents is due to the eigenstate components not being identically distributed. In Sec. IV B we present data showing that this is not the reason for the anomalous scaling of EEV fluctuations.

These results show that the nonergodic scaling must be due to correlations present in the eigenstates. In Sec. IV C we examine the simplest (and most prominent) type of correlations between eigenstate coefficients, namely, those captured in the covariance matrix. Perhaps surprisingly, we find that these correlations do not explain the anomalous scaling either. The anomalous scaling exponent for $k = 3$ EEV fluctuations is thus caused by more subtle (higher-order) correlations.

A. Participation ratios

For this subsection it will be convenient to consider our operator A to be Hermitian. We expand the eigenstates $|E_\alpha\rangle$ of the Hamiltonian in the eigenstate basis $|\phi_\gamma\rangle$ of the operator A

$$|E_\alpha\rangle = \sum_\gamma c_\gamma^{(\alpha)} |\phi_\gamma\rangle, \tag{13}$$

where $c_\gamma^{(\alpha)} = \langle \phi_\gamma | E_\alpha \rangle$. If we denote the eigenvalues of A as a_γ, then the EEVs can be written as

$$A_{\alpha\alpha} = \sum_{\gamma=1}^{D} \left| c_\gamma^{(\alpha)} \right|^2 a_\gamma. \tag{14}$$

We regard the coefficients $c_\gamma^{(\alpha)}$ to be random variables, with each eigenstate index (α) denoting a different sample from the same underlying distribution. The distribution is assumed to be the same for every γ. As usual, this framework will not capture large-scale dependencies of the EEVs $A_{\alpha\alpha}$ on the energies E_α. This is acceptable because we are interested in the fluctuations only.

The variance of the EEVs is

$$\begin{aligned} \mathrm{var}\left(\sum_{\gamma=1}^{D} |c_\gamma|^2 a_\gamma \right) &= \sum_{\gamma=1}^{D} \mathrm{var}(|c_\gamma|^2) a_\gamma^2 \\ &= \mathrm{var}(|c_\gamma|^2)\, \mathrm{tr}(A^2). \end{aligned} \tag{15}$$

The variance of $|c_\gamma|^2$ can be written as

$$\mathrm{var}(|c_\gamma|^2) = E[|c_\gamma|^4] - (E[|c_\gamma|^2])^2 = \frac{1}{DP} - \frac{1}{D^2}, \tag{16}$$

where we have used the definition of the participation ratio to be

$$P_\alpha = \left(\sum_{\gamma=1}^{D} \left| c_\gamma^{(\alpha)} \right|^4 \right)^{-1} = \left(D \times E\left[\left| c_\gamma^{(\alpha)} \right|^4 \right] \right)^{-1}. \tag{17}$$

We thus have the prediction for the EEV variance

$$\sigma^2 = \left(\frac{1}{DP} - \frac{1}{D^2} \right) \mathrm{tr}(A^2) = \left(\frac{1}{DP} - \frac{1}{D^2} \right) \mathrm{tr}(AA^\dagger) \tag{18}$$

for Hermitian operators. For *Gaussian* states, $P = D/3$, so that this expression for σ^2 reduces to Eq. (7). More generally, as long as the participation ratio scales linearly with D, the factor in brackets $\sim 1/D^2$, so that we obtain the same scaling as for Gaussian states. For nonergodic states $P \sim D^K$ with $K < 1$, the first term in brackets would dominate and one would obtain different scaling.

In Fig. 5 we show the behavior of the participation ratio in the basis of eigenstates of $(a_2^\dagger a_1 + a_1^\dagger a_2)$. The midspectrum P_α is close to the Gaussian expectation for highly chaotic (larger k) systems. For $k = 3$ the deviation from Gaussianity ($P = D/3$) is strong. However, in both cases the scaling of P_α with Hilbert space dimension D is very linear (lower panels).

Thus, Hilbert space occupancy does not explain the observed anomalous exponent of EEV fluctuations.

B. Nonidentical distribution of eigenstate coefficients

The analysis in Secs. IV A and III A are based on eigenstate coefficients being *identically distributed* and *independent*.

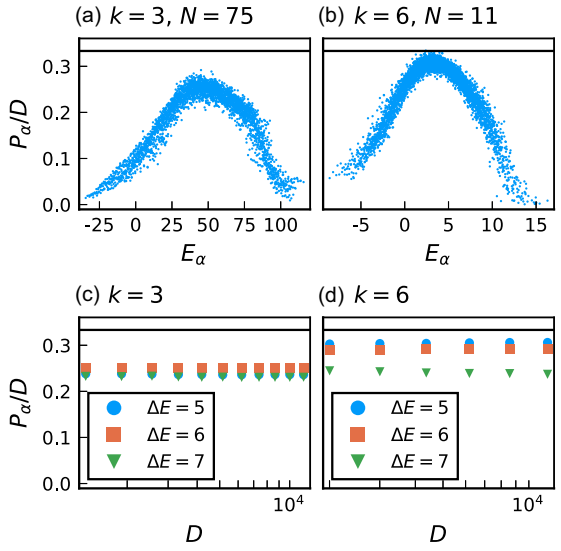

FIG. 5. Participation ratio in the basis of eigenstates of the operator $a_2^\dagger a_1 + a_1^\dagger a_2$. Horizontal lines indicate the Gaussian expectation ($= \frac{1}{3}$). Top panels: Normalized participation ratio P_α/D of energy eigenstates, versus corresponding energy eigenvalues. Lower panels: average normalized participation ratio for different energy intervals plotted against Hilbert space dimension D, for fixed chain length k and increasing particle number N.

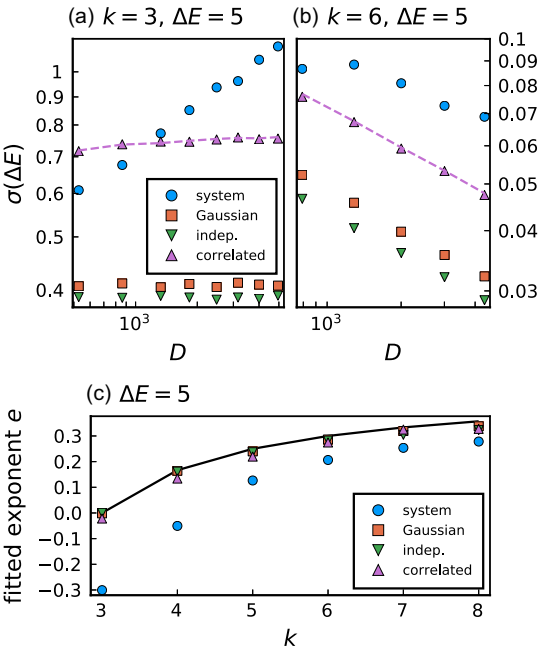

FIG. 6. The operator in all plots is $a_2^\dagger a_1$. Blue dots: eigenstates of physical Bose-Hubbard system. Red squares: Gaussian states with i.i.d. components. Green down triangles: vectors with independent but nonidentically distributed components, each component sampled from system eigenstates. Purple up triangles: multivariate Gaussian states with covariance matrix estimated from system eigenstates. (a), (b) EEV fluctuations. The dashed purple line is the prediction by Eq. (20). (c) The exponent e, such that $\sigma \sim D^{-e}$, versus the number of sites k for the same distributions as in panels (a), (b).

Could it be that the failure to capture the EEV fluctuation scaling at small k results from the eigenstate components having nonidentical distributions?

To check, we drop the condition that the eigenstates have identically distributed components and only assume that the components are independent. In Fig. 6 we show the EEV fluctuations obtained from an estimation of the underlying distributions of the eigenstate components of the Bose-Hubbard systems. We sampled uniformly from components of all eigenstates of the Bose-Hubbard model in a specific energy interval. Effectively, for each component of the state, we randomly picked an eigenstate in the energy interval and used the entry of the corresponding component. The EEV fluctuations are then calculated from such sampled states. The resulting data are marked "independent" in Fig. 6. The results match well with the EEV fluctuations obtained from Gaussian states and do not match the EEV fluctuations of the actual physical systems for small k.

We conclude that any model for the wave functions with independent components does not explain the observed anomalous scaling at small k. In other words, the root cause of the phenomenon is not the eigenstate coefficients having nonidentical or non-Gaussian distributions, or insufficient occupancy of the Hilbert space. Rather, we have traced the cause to the fact that the eigenstate coefficients are not independent.

C. Eigenstate Correlations

Continuing our effort to identify what feature of small-k eigenstates is responsible for the anomalous ETH scaling, we relax the constraints on the model states even further. Now, we assume that eigenstates are drawn independently from a multivariate distribution Z, but the D components of Z are allowed to be correlated. Given a multivariate distribution Z, the statistical correlations between components are quantified by the covariance matrix Σ. The covariance matrix in the case of eigenstates can be estimated by regarding the eigenstates within a specific energy interval as different samples of Z.

It is reasonable to assume that the mean of all components of Z is zero, as components of midspectrum eigenstates generally have zero mean. Then an estimate of Σ is given by

$$\Sigma = N_{\Delta E}^{-1} \sum_{E_\alpha \text{ in } \Delta E} |E_\alpha\rangle\langle E_\alpha|, \tag{19}$$

where E_α and $|E_\alpha\rangle$ denote eigenvalues and eigenstates, respectively, and $N_{\Delta E}$ is the number of eigenstates in the energy window ΔE. Eq. (19) follows directly from the definition of the sample covariance matrix of Z, where the samples are the eigenstates $|E_\alpha\rangle$.

In Appendix C, Fig. 9, we have provided visualizations of estimated covariance matrices for $k = 3$ and $k = 6$. The $k = 3$ case is seen to have significant off-diagonal elements (arranged in intriguing patterns), indicating nonnegligible correlations between the eigenstate components.

Once we have constructed the correlation matrix Σ from the actual eigenstates, we can sample D-component vectors whose components have a Gaussian distribution and are correlated according to the matrix Σ. In Fig. 6 the EEV fluctuations obtained from such sampled states are marked as "correlated." The values of the fluctuations thus obtained are larger

than those obtained from the independent-component random states, and more comparable to the fluctuations obtained from the physical eigenstates. In the chaotic cases (large k), all of these cases have the same scaling. However, in the $k = 3$ case, the scaling exponent is close to the ergodic (Gaussian) case and does not reproduce the anomalous scaling at all. This is seen Figs. 6(a) and 6(c), where the fitted exponents are plotted. The fitted exponent is slightly off the Gaussian value for small k, but far from the anomalous values of the physical system.

These results show that the deviation of the physical system from expected 'ergodic' behavior is only partially captured by the two-point correlations between the eigenstate components. This suggests that the small-k eigenstates deviate from randomness in some more drastic manner, which does not seem easy to quantify.

In addition to the direct numerical verification discussed above, one can use analytic results to argue (nonrigorously) that inclusion of reasonable two-point correlations in the model of random states should not change the EEV fluctuation scaling exponent. Given a multivariate Gaussian distribution with mean zero and covariance matrix Σ, we can show (details in Appendix D) that the variance of EEV fluctuations is given by

$$\mathrm{var}(\langle A\rangle) = \frac{1}{D^2}[\mathrm{tr}((D\Sigma A)^2) + \mathrm{tr}(D\Sigma A D\Sigma A^t)]. \qquad (20)$$

This is Eq. (7) with the change $A \to D\Sigma A$. The variance of components of the wave function is not fixed by normalization of the eigenstates any more. But it is reasonable to assume that it still scales as $\sim 1/D$, and we have checked numerically that this scaling holds for the midspectrum eigenstates of all our physical systems, including $k = 3$. Since the variances of the wave function components are the diagonal entries of Σ, the diagonals of $D\Sigma$ scale (at most) as constant in D. By the Cauchy-Schwartz theorem the off-diagonal terms of Σ are bounded by the diagonal, so *every* component of $D\Sigma$ is (at most) constant in D.

Without making assumptions about the detailed structure of Σ, we cannot derive rigorously the scaling of the traces in Eq. (20), which was possible for Eq. (8) or Eq. (9). However, since $D\Sigma$ is elementwise at most $\sim D^0$, and assuming Σ is not too exotic, one can argue that the derivation in Appendix E should hold for this case as well. In other words, for "reasonable" Σ, one expects the same scaling as in the case of independent Gaussian eigenstates. This is consistent with Fig. 6, where the matrix Σ is estimated numerically from the physical eigenstates.

V. DISCUSSION AND CONTEXT

Motivated by questions relating quantum dynamics to statistical mechanics, we have undertaken a study of the eigenstate thermalization hypothesis in the scaling sense, but considering increasing Hilbert space dimensions along the (semi)classical limit rather than the usual thermodynamic limit. This has led to a characterization of the distinctive properties of few-site Bose-Hubbard systems in terms of anomalous scaling exponents.

A. Summary of analytic results

For GOE eigenstates, i.e., states whose components can be approximated by Gaussian-distributed random variables, we have used trace expressions for the EEV fluctuation σ, Eq. (7). For operators of the type $A = a_j^\dagger a_i$, the trace operators can be expressed as Eq. (8). Based on these main expressions, we are able to predict ideal scaling behaviors of EEV fluctuations in the classical limit, for both unnormalized operators of the type A and normalized operators $\bar{A} = A/N$. Of course, the usual ETH scaling of the thermodynamic limit also follows from these expressions.

In the classical limit $N \gg k$, the EEV fluctuations are found for such idealized eigenstates to behave as $\sigma \sim D^{-e_0}$, with $e_0 = \frac{1}{2} - \frac{1}{(k-1)}$ for unnormalized A operators and $e_0 = 1/2$ for normalized $\bar{A}$ operators.

In addition, we have presented expressions for σ for a number of related cases, e.g., for i.i.d. distributed eigenstate components with the distribution not assumed to be Gaussian, Eq. (6), in terms of the participation ratio, Eq. (18), and for the more general case where the eigenstate components are allowed to be correlated according to a covariance matrix, Eq. (20).

B. Summary of numerical results

We have explored the scaling exponent for various lattice lengths k, increasing the boson number N with fixed k to approach the classical limit. At larger k, the exponent matches the random-eigenstate prediction. At small k, the fluctuation appears to have power-law dependence $\sigma \sim D^{-e}$ on the Hilbert space dimension, i.e., e is well-defined, but the value of e differs markedly from the ergodic prediction. Through a series of additional numerical tests, we have shown that this anomalous scaling is not explained by two-point correlations between eigenstate components.

The small-size Bose-Hubbard systems thus have midspectrum eigenstates which violate the usual randomness approximation in some subtle higher-order manner.

C. Deviation from Ergodicity

The deviation of quantum many-body systems from ergodicity has been the subject of interest from multiple viewpoints in recent years. Other than the strong violations of ETH/ergodicity due to integrability or many-body localization [33,96], more subtle departures have also been addressed or observed. For example, some otherwise chaotic systems display "many-body scars" [97], an exponentially small fraction of eigenstates possessing integrablelike properties. In addition, in many-body systems that are nominally chaotic, midspectrum states are largely well-modeled by random states, but small or subleading deviations have been observed in various properties [20,37,45,86–91]. However, *scaling* properties in these systems generally follow random-state predictions. In the small-k Bose-Hubbard systems, we have shown a striking exception: a system which is not integrable or many-body localized, but nevertheless violates the usual scaling behavior expected in chaotic systems.

The three-site and four-site Bose-Hubbard systems are widely known to be imperfectly chaotic, in particular because

their classical phase space has been explored and is known to have both chaotic and regular regions [53,72,76–81]. With the current interest in chaos in many-body eigenstates, it is important to characterize such deviations from chaoticity. In this work, ETH scaling (i.e., the scaling of EEV fluctuations) has turned out to be fruitful approach to characterize these special systems.

D. Open questions and ideas arising from this work

The present work opens up a number of new questions deserving investigation:

(1) We have found that the small-k Bose-Hubbard systems display EEV fluctuations scaling with exponents that appear numerically well-defined but very clearly different from the random-state prediction. An analytic explanation for these observed new exponents is currently not available, and remains an open question. The anomalous scaling is related to the insufficient chaoticity of few-site systems, which is closely connected to the mixed phase space of the corresponding classical system. Hence a tempting conjecture is that some property measuring the degree of chaos in the classical limit might explain the exponents.

(2) Our analytic results have focused on essentially infinite-temperature states. It would be interesting to develop trace expressions for finite temperatures. This is likely not possible to do in complete generality without making assumptions on the system Hamiltonian, but perhaps some results can be derived with minimal assumptions, such as locality of the Hamiltonian.

(3) For the thermodynamic limit, the EEV fluctuations of *integrable* systems generally show power-law scaling in N or k [11,13–19], which translates into $\sim \ln D$ scaling. For the classical limit, however, power-law scaling in N would mean power-law scaling in D as well. Our numerics (Appendix B) shows that fitting $\sigma \sim D^{-e}$ in the integrable regime yields $e = -1/(k-1)$ for A-type operators and $e = 0$ for $\bar{A}$-type operators. A detailed understanding and explanation of these exponents remains a task for future research.

(4) Bose-Hubbard systems are, of course, not the only quantum systems with a classical limit. It remains to be discovered how generic our findings are. Comparing chaos-related properties between quantum systems and the corresponding classical systems has also been of interest in few-spin systems [98–109] and in spin-boson systems [106,107,110–119]. (The classical system is obtained in the limit of large spin quantum number.) Studying the behavior of EEV fluctuations in such systems when approaching the classical limit would provide interesting characterizations of ergodicity, e.g., of how well randomness approximations work.

(5) As part of our effort to address the anomalous scaling at small k, we have briefly examined the covariance matrix of eigenstates, treating each eigenstate as a sample drawn from the distribution of eigenstates, according to Eq. (19). Studying the thus-defined covariance matrix might be fruitful for various quantum systems, as the departure of this matrix from the identity matrix tells us how different the eigenstates are from infinite-temperature states. A further significance of this covariance matrix is that the same object is the microcanonical density matrix, and hence its structure should provide insights into the connection betwen quantum eigenstates and thermodynamics.

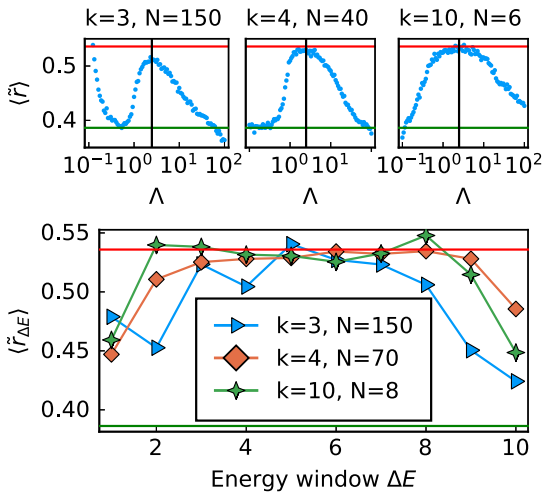

FIG. 7. Top: Level ratios $\tilde{r}$ averaged over the whole spectrum, as a function of interaction strength $\Lambda = UN$, shown in the range $\Lambda \in (0.1, 100)$. The horizontal lines are $\langle\tilde{r}\rangle_{\text{integr}}$ (lower green) and $\langle\tilde{r}\rangle_{\text{GOE}}$ (upper red). The vertical line indicates $\Lambda = 10^{13/33} \approx 2.477$. Bottom: Mean level ratio against ten evenly spaced energy windows ΔE, labeled 1 through 10 and plotted against these labels, for $\Lambda \approx 2.477$, various system sizes. The match to the GOE value is better away from spectral edges.

ACKNOWLEDGMENTS

M.H. thanks P. Ribeiro and R. Mondaini for enlightening discussions. We thank J. D. Urbina and K. Richter for useful correspondence. Some computations were performed on the Irish Center for High-End Computing. G.N. is supported by the Irish Research Council Government of Ireland Postgraduate Scholarship Scheme (Grant No. GOIPG/2019/58).

APPENDIX A: LEVEL SPACING STATISTICS

The distribution of energy eigenvalue spacings, $s_\alpha = E_{\alpha+1} - E_\alpha$ for ordered $E_\alpha < E_{\alpha+1}$, is often used as an indicator for quantum chaos. Measuring this distribution involves unfolding the spectrum. This is bypassed by investigating the distribution of spacing ratios [120,121],

$$r_\alpha = \frac{s_{\alpha+1}}{s_\alpha} \quad \text{and} \quad \tilde{r}_\alpha = \min\left(r_\alpha, \frac{1}{r_\alpha}\right).$$

The latter has the advantage that it is bounded. Quantum Hamiltonians are considered chaotic when the distributions follow that of the relevant Wigner-Dyson ensemble, which in our case is the GOE ensemble. The mean $\tilde{r}$ for GOE is $\langle\tilde{r}\rangle_{\text{GOE}} \approx 4 - 2\sqrt{3} \approx 0.53590$. For an integrable Hamiltonian, the level spacing distribution is Poissonian (exponential); this leads to $\langle\tilde{r}\rangle_{\text{integr}} = 2\log 2 - 1 \approx 0.38629$.

Figure 7 (top) shows that, with increasing interaction strength $\Lambda = UN$, the Bose-Hubbard systems turn from integrable to chaotic and back to integrable. Some anomalies are visible for short chains (small k). First, the distributions of the

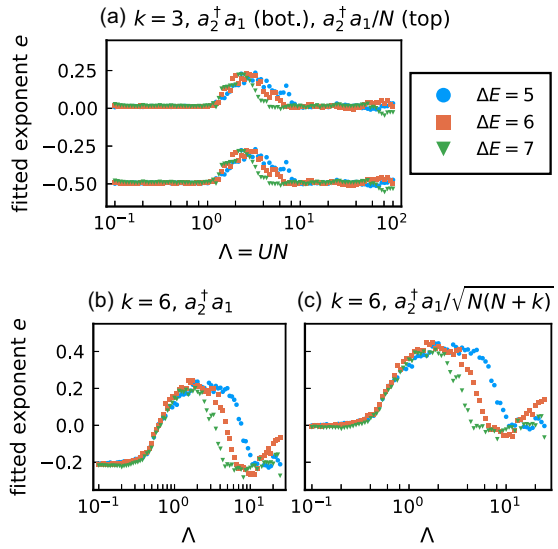

FIG. 8. Exponent e obtained from $\sigma \sim D^{-e}$ fits, as a function of the interaction parameter $\Lambda = UN$. Results are shown for both unnormalized operator $A = a_2^\dagger a_1$ and its normalized version $\bar{A}$, with $\bar{A} = A/N$ for the $k = 3$ system (top) and $\bar{A} = A/\sqrt{N(N+k)}$ for the $k = 6$ system (bottom).

level ratios for very small Λ or very large Λ match neither GOE nor Poisson statistics. Also, for small k, in the most chaotic regime, the peak of $\langle \tilde{r} \rangle$ is still noticeably lower than the GOE value ≈0.534. As k increases, the peak gets closer and closer to the GOE value, consistent with the intuition that larger-k chains are more chaotic.

Our grid of Λ values contains 100 values spaced logarithmically from 0.1 to 100. Among these values, $\Lambda = 10^{13/33} \approx 2.477$ is found to be close to the location of the chaotic peak, for all k. Therefore, in this work we have shown data for this value of the interaction parameter.

Of course, we do not expect that the full spectrum obeys GOE statistics—the spectral edges are expected to deviate. This can be observed in Eq. (7) (bottom panel), where we plot $\langle \tilde{r} \rangle$ against different energy windows.

APPENDIX B: DEPENDENCE OF EEV SCALING ON INTERACTION STRENGTH Λ

In the main text we focused on the value of the interaction parameter $\Lambda = UN$ at which our systems are most chaotic. Here, we show how changing Λ affects the scaling of EEV fluctuations. Fitting the fluctuation data to $\sigma \sim D^{-e}$, we extract exponents e which we show in Fig. 8 as a function of Λ. We compare the smallest Bose-Hubbard chain with $k = 3$ sites with a larger, thus more chaotic chain with $k = 6$.

We show data both for the operator $A = a_2^\dagger a_1$ and the normalized operator $\bar{A} \approx a_2^\dagger a_1/N$. For $k = 3$, we show results for $\bar{A} = a_2^\dagger a_1/N$. (As the data for small k extends into the $N \gg k$ regime, it is reasonable to approximate $\sqrt{N(N+k)} \approx N$.) For larger k values, the regime $N \gg k$ is difficult to reach numerically. Therefore, it is appropriate to normalize with the factor $\sqrt{N(N+k)}$ instead of the factor N, as the approximation $\sqrt{N(N+k)} \approx N$ made for Eq. (8) or Eq. (E9) may not be accurate.

Since $N \sim D^{1/(k-1)}$, the exponent e for $\sigma(\bar{A})$ is shifted upwards compared to that for $\sigma(A)$ by $1/(k-1)$. This is seen in Fig. 8 for both $k = 3$ (shift of $\frac{1}{3-1} = 0.5$) and for $k = 6$ (shift of $\frac{1}{6-1} = 0.2$).

At intermediate values of Λ, when the system is (partially) chaotic, the value of e is near that discussed in the main text. If we had fully chaotic (Gaussian) eigenstates, then we would expect $e = 0.5$ for the normalized operators $\bar{A}$ and $e = 0.5 - 0.5 = 0$ ($k = 3$) or $e = 0.5 - 0.2 = 0.3$ ($k = 6$) for the unnormalized operators A. Compared to the Gaussian prediction, the observed exponents are significantly smaller for the $k = 3$ system, and somewhat smaller for the $k = 6$ system, as discussed in detail in the main text.

For small or large Λ, the system is (near-)integrable. In these limits, the fluctuations for normalized operators $\bar{A}$ do not have power-law dependence on D, and the fit to D^{-e} results in $e = 0$. Thus, eigenstate fluctuation scaling of *normalized* operators $\bar{A} = A/N$ in the classical limit is analogous to that of *local* operators in the thermodynamic limit: $e \to 0$ in the integrable limits and $e \approx 0.5$ in the chaotic regime [11]. For local operators in the thermodynamic limit, the fluctuations have power-law dependence on system size [11,13–19], i.e., logarithmic dependence on D. A detailed study of the (near-)integrable models in the classical limit remains an interesting task for future studies.

Because e for $\bar{A}$ settles to zero for $\Lambda \to 0$ and $\Lambda \to \infty$, the exponent for the normalized operator $A = a_2^\dagger a_1$ settles to $-1/(k-1)$ in these limits, i.e., to -0.5 for the trimer and to -0.2 for $k = 6$. This is clearly seen in Fig. 8.

APPENDIX C: ESTIMATED COVARIANCE MATRICES FROM PHYSICAL EIGENSTATES

In Sec. IV C we discussed results incorporating the two-point correlations between eigenstate components, as embodied in the covariance matrix. The covariance matrix for physical midspectrum eigenstates is calculated according to Eq. (19), i.e., as an equal-weight mixture of the density matrices $|E_\alpha\rangle\langle E_\alpha|$ corresponding to each eigenstate in the energy window. Here we show the structure of the covariance matrices obtained in this way, i.e., we visualize the two-point correlations present in the physical eigenstates.

To visualize the structure of covariance matrices one has to fix a basis of the Hilbert space. In Fig. 9 we show covariance matrices with respect to the defining basis $\mathcal{B}$. The elements of $\mathcal{B}$ are the mutual eigenstates of all number operators $n_j = a_j^\dagger a_j$, denoted by $|n_1, \ldots, n_k\rangle$ where $n_1 + \cdots + n_k = N$. For two states $|\psi\rangle = |n_1, \ldots, n_k\rangle$ and $|\phi\rangle = |m_1, \ldots, m_k\rangle$ we say that $|\psi\rangle < |\phi\rangle$ if and only if the states interpreted as $(N+1)$-adic numbers satisfy $(\psi)_{N+1} < (\phi)_{N+1}$, i.e.,

$$|\psi\rangle < |\phi\rangle \iff \sum_{j=1}^{k} n_j (N+1)^j < \sum_{j=1}^{k} m_j (N+1)^j. \quad \text{(C1)}$$

The basis states in $\mathcal{B}$ are in descendent order with respect to the ordering given by Eq. (C1). For example, for $k = 3$ and

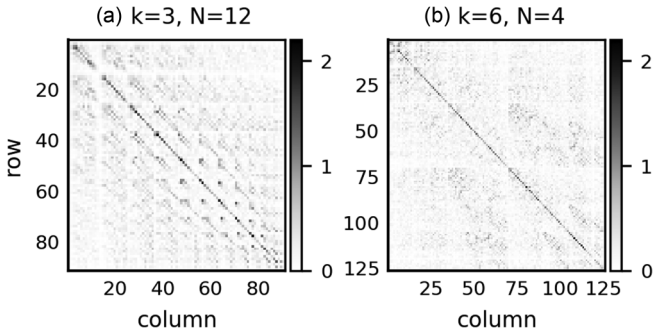

FIG. 9. Normalized estimated covariance matrix $D\Sigma$ of midspectrum eigenstates (energy window $\Delta E = 5$) for Bose-Hubbard chains with k sites and N particles. The estimate Σ is defined in Eq. (19). The absolute values of matrix entries, $|D \cdot \Sigma_{ij}|$, corresponding to basis $\mathcal{B}$ described in text, are shown. The tick labels are row and column indices, e.g., in the top left is the entry $|D \cdot \Sigma_{11}|$. N had to be chosen significantly smaller than in the rest of the paper to visualize the patterns without zooming. The patterns are stable for increasing N.

$N = 2$, $\mathcal{B}$ is ordered as

$$\mathcal{B} = (|0,0,2\rangle, |0,1,1\rangle, |0,2,0\rangle, |1,0,1\rangle, |1,1,0\rangle, |2,0,0\rangle). \tag{C2}$$

If the components of eigenstates of Bose-Hubbard chains would be independent, then their estimated covariance matrix would be close to the identity matrix. Figure 9 shows that, even for $k = 6$, there are significant off-diagonal terms, indicating that the eigenstate components are not independent. The deviation from the identity matrix suggests that the midspectrum states deviate from infinite-temperature states, even for significantly chaotic states, consistent with Refs. [20,37,45,86–91]. For small k, nonzero off-diagonal elements are even more pronounced, and these appear in intricate patterns [Fig. 9(a)].

APPENDIX D: VARIANCE AND COVARIANCE OF EEVS OF RANDOM EIGENSTATES

In this section, we provide derivations of some of the equations that were announced and used in the main text without proof. First, we derive the results announced in Section III for random eigenstates with independent and identically distributed (i.i.d.) components (Sec. D 1). Next, we prove the result Eq. (20), announced in Sec. IV C, for random vectors whose components are not independent, with two-point correlations described by a covariance matrix (Sec. D 2).

1. Random vectors with i.i.d. components

Let A be a $D \times D$ square matrix and Z be a D-dimensional, multivariate random state with identically and independently distributed components Z_i, each with mean 0. The statistical variance of $\langle A\rangle = \langle Z|A|Z\rangle$ is given by

$$\mathrm{var}(\langle A\rangle) = \sum_{i,j,i',j'=1}^{D} A_{i,j}A_{i',j'}\,\mathrm{cov}(Z_iZ_j, Z_{i'}Z_{j'}), \tag{D1}$$

where

$$\begin{aligned}\mathrm{cov}(Z_iZ_j, Z_{i'}Z_{j'}) &= E[Z_iZ_jZ_{i'}Z_{j'}] - E[Z_iZ_j]\cdot E[Z_{i'}Z_{j'}]\\ &= E[Z_iZ_jZ_{i'}Z_{j'}] - \delta_{ij}\delta_{i'j'}E\left[Z_i^2\right]^2.\end{aligned} \tag{D2}$$

By the independence of Z_i, Z_j for $i \neq j$, $E[Z_iZ_jZ_{i'}Z_{j'}]$ is only nonzero if there is no index i, j, i', j' different to the other three. The only possibilities for this are

$$\begin{aligned} &i = j = i' = j',\\ &i = j \text{ and } i' = j',\\ &i = i' \text{ and } j = j',\\ &i = j' \text{ and } j = i',\end{aligned} \tag{D3}$$

so

$$\begin{aligned}E[Z_iZ_jZ_{i'}Z_{j'}] = \delta_{ij}\delta_{ii'}\delta_{ij'}E\left[Z_i^4\right] &+ (1-\delta_{ij}\delta_{ii'}\delta_{ij'})\\ &\times\left[\delta_{ij}\delta_{i'j'}E\left[Z_i^2\right]^2 + \delta_{ii'}\delta_{jj'}E\left[Z_i^2\right]^2\right.\\ &\left.+\,\delta_{ij'}\delta_{ji'}E\left[Z_i^2\right]^2\right].\end{aligned} \tag{D4}$$

Then we get

$$\begin{aligned}\mathrm{var}(\langle A\rangle) = E\left[Z_1^4\right]\sum_i A_{ii}^2 &+ E\left[Z_1^2\right]^2\\ &\times\left[\sum_{i\neq i'}A_{ii}A_{i'i'} + \sum_{i\neq j}A_{ij}^2 + \sum_{i\neq j}A_{ij}A_{ji}\right]\\ &- E\left[Z_1^2\right]^2\sum_{i,i'}A_{ii}A_{i'i'}\end{aligned} \tag{D5}$$

and

$$\begin{aligned}\mathrm{var}(\langle A\rangle) &= \left(E\left[Z_1^4\right] - E\left[Z_1^2\right]^2\right)\sum_i A_{ii}^2\\ &\quad + E\left[Z_1^2\right]^2\left[\sum_{i\neq j}A_{ij}^2 + \sum_{i\neq j}A_{ij}A_{ji}\right]\\ &= \left(E\left[Z_1^4\right] - 3E\left[Z_1^2\right]^2\right)\sum_i A_{ii}^2\\ &\quad + E\left[Z_1^2\right]^2[\mathrm{tr}(A^2) + \mathrm{tr}(AA^\dagger)].\end{aligned} \tag{D6}$$

This is Eq. (6) of the main text. It is a rather general result, not assuming a particular distribution of the components, only that they should be independent and identically distributed and have mean 0.

Now, we specialize to the case that the components Z_i are each normally distributed with mean 0 and variance $1/D$. Then

$$E\left[Z_i^2\right] = \frac{1}{D}E[(\sqrt{D}Z_i)^2] = \frac{1}{D} \tag{D7}$$

and

$$E\left[Z_i^4\right] = \frac{1}{D^2}E[(\sqrt{D}Z_i)^4] = \frac{3}{D^2}, \tag{D8}$$

because $\sqrt{D}Z_i$ is normally distributed with mean 0 and variance 1. Plugging this into the above formula,

we get

$$\mathrm{var}(\langle A\rangle) = \left(\frac{3}{D^2} - \frac{3}{D^2}\right)\sum_i A_{ii}^2 + \frac{1}{D^2}[\mathrm{tr}(A^2) + \mathrm{tr}(AA^\dagger)t] \tag{D9}$$

$$= \frac{1}{D^2}[\mathrm{tr}(A^2) + \mathrm{tr}(AA^\dagger)]. \tag{D10}$$

This concludes the proof of Eq. (7).

2. Including two-point correlations

We now relax the assumption of independence and allow the wave function components to have two-point correlations. The trace expression in this case is Eq. (20), which we will now prove.

Assume $Z = LX$, where X is a vector whose independent components are Gaussian-distributed with mean zero and variance 1, and L is the Cholesky root of a nonrandom $D \times D$ (covariance-) matrix Σ, i.e., $\Sigma = LL^t$. Then Z has mean zero and the covariances between components of Z are given by Σ. We compute the statistical variance of the EEVs as

$$\begin{aligned}\mathrm{var}(\langle A\rangle) &= \mathrm{var}((LX)^t ALX)\\ &= \mathrm{var}(X^t L^t ALX)\\ &= \mathrm{var}(1/\sqrt{D}X^t DL^t AL1/\sqrt{D}X).\end{aligned} \tag{D11}$$

Because the components of $1/\sqrt{D}X$ are normally distributed with mean 0 and variance $1/D$, we can use Eq. (7) with A replaced by $L^t AL$. This leads to

$$\begin{aligned}\mathrm{var}(\langle A\rangle) &= \frac{1}{D^2}(\mathrm{tr}(D^2(L^t AL)^2) + \mathrm{tr}(D^2 L^t AL(L^t AL)^t)\\ &= \frac{1}{D^2}(\mathrm{tr}((D\Sigma A)^2) + \mathrm{tr}(D\Sigma AD\Sigma A^t),\end{aligned} \tag{D12}$$

which concludes the proof of Eq. (20).

APPENDIX E: SCALING OF OPERATORS

In this section we derive results announced in the main text concerning the scaling of the traces. For $A = a_j^\dagger a_i$ we prove the trace expression of Eq. (8). For the classical limit, we prove the scaling relation, Eq. (9), for A being a (finite) linear combination of terms of the type $a_j^\dagger a_i$.

Considering A to be such a linear combination, A^2 and $A^\dagger A$ can be written as a sum of terms $a_j^\dagger a_i a_{j'}^\dagger a_{i'}$. Consider a defining basis state $|\psi\rangle = |n_1, \ldots, n_k\rangle$, which has n_j particles on site j. Then

$$a_j^\dagger a_i|\psi\rangle = \delta_{ij} n_i|\psi\rangle + (1-\delta_{ij})\sqrt{n_j+1}\sqrt{n_i}|\ldots, n_i - 1, n_j + 1, \ldots\rangle. \tag{E1}$$

Using Eq. (E1) twice we get

$$\langle\psi|a_j^\dagger a_i a_{j'}^\dagger a_{i'}|\psi\rangle = \delta_{i'j'}\delta_{ij} n_{i'} n_i + (1-\delta_{i'j'})(1-\delta_{ij})\delta_{ij'}\delta_{ji'}(n_{j'}+1)n_{i'}. \tag{E2}$$

Now we will calculate $\mathrm{tr}(a_j^\dagger a_i a_{j'}^\dagger a_{i'})$. First, let $i = j = i' = j'$. Using that there are $\binom{N-l+k-2}{k-2}$ states with l particles on site i, we get

$$\mathrm{tr}\left(n_i^2\right) = \sum_{l=0}^{N} l^2 \binom{N-l+k-2}{k-2}. \tag{E3}$$

Writing l^2 in terms of binomial coefficients and exploiting an upper index Vandermonde identity, namely,

$$\sum_{l=0}^{n}\binom{l}{c_1}\binom{n-l}{c_2} = \binom{n+1}{c_1+c_2+1}, \tag{E4}$$

for constants n, c_1 and c_2, we get

$$\mathrm{tr}\left(n_i^2\right) = \frac{N(2N+k-1)}{k(k+1)}D. \tag{E5}$$

Now let $i = j$ and $i' = j'$ but $i \neq i'$. There are $\binom{N-l-s+k-3}{k-3}$ many states with l particles on site i and s particles on site i', so

$$\mathrm{tr}(n_i n_{i'}) = \sum_{l=0}^{N}\sum_{s=0}^{N-l} ls\binom{N-l-s+k-3}{k-3}. \tag{E6}$$

Invoking the Vandermonde identity Eq. (E4) twice gives us

$$\mathrm{tr}(n_i n_{i'}) = \frac{N(N-1)}{(k+1)k}D. \tag{E7}$$

The case $i \neq j$ and $i' \neq j'$, but $j = i'$ and $i = j'$, works exactly the same as $i = j$ and $i' = j'$ but $i \neq i'$. Using Eq. (E4) twice on

$$\mathrm{tr}(a_j^\dagger a_i a_i^\dagger a_j) = \sum_{l=0}^{N}\sum_{s=0}^{N-l}(l+1)s\binom{N-l-s+k-3}{k-3} \tag{E8}$$

results in

$$\mathrm{tr}(a_j^\dagger a_i a_i^\dagger a_j) = \frac{N(N+k)}{k(k+1)}D. \tag{E9}$$

In the classical limit, $k \ll N$, Eqs. (E5), (E7), and (E9) all scale as $\sim N^2 D$, so the corresponding trace expressions of all typical observables scale as

$$\mathrm{tr}(A^2) + \mathrm{tr}(A^\dagger A) \sim N^2 D. \tag{E10}$$

In the thermodynamic limit, $k = \rho N$ for a density ρ not depending on N nor k and $k, N \to \infty$, the trace expressions scale as

$$\mathrm{tr}(A^2) + \mathrm{tr}(A^\dagger A) \sim D, \tag{E11}$$

because the leading order of k and N is quadratic in both the numerators and the denumerators in Eqs. (E5), (E7), and (E9). By combining this with the results in Appendix D we rediscover the $D^{-1/2}$ dependence of the EEV fluctuations in the thermodynamic limit for Gaussian states and observables A.

[1] J. M. Deutsch, Quantum statistical mechanics in a closed system, Phys. Rev. A **43**, 2046 (1991).

[2] M. Srednicki, Chaos and quantum thermalization, Phys. Rev. E **50**, 888 (1994).

[3] M. Srednicki, Thermal fluctuations in quantized chaotic systems, J. Phys. A: Math. Gen. **29**, L75 (1996).

[4] M. Srednicki, The approach to thermal equilibrium in quantized chaotic systems, J. Phys. A: Math. Gen. **32**, 1163 (1999).

[5] M. Rigol, V. Dunjko, and M. Olshanii, Thermalization and its mechanism for generic isolated quantum systems, Nature **452**, 854 (2008).

[6] A. Polkovnikov, K. Sengupta, A. Silva, and M. Vengalattore, Colloquium: Nonequilibrium dynamics of closed interacting quantum systems, Rev. Mod. Phys. **83**, 863 (2011).

[7] M. Rigol and M. Srednicki, Alternatives to Eigenstate Thermalization, Phys. Rev. Lett. **108**, 110601 (2012).

[8] J. Eisert, M. Friesdorf, and C. Gogolin, Quantum many-body systems out of equilibrium, Nat. Phys. **11**, 124 (2015).

[9] L. D'Alessio, Y. Kafri, A. Polkovnikov, and M. Rigol, From quantum chaos and eigenstate thermalization to statistical mechanics and thermodynamics, Adv. Phys. **65**, 239 (2016).

[10] C. Neuenhahn and F. Marquardt, Thermalization of interacting fermions and delocalization in fock space, Phys. Rev. E **85**, 060101(R) (2012).

[11] W. Beugeling, R. Moessner, and M. Haque, Finite-size scaling of eigenstate thermalization, Phys. Rev. E **89**, 042112 (2014).

[12] W. Beugeling, R. Moessner, and M. Haque, Off-diagonal matrix elements of local operators in many-body quantum systems, Phys. Rev. E **91**, 012144 (2015).

[13] S. Ziraldo and G. E. Santoro, Relaxation and thermalization after a quantum quench: Why localization is important, Phys. Rev. B **87**, 064201 (2013).

[14] T. N. Ikeda, Yu Watanabe, and M. Ueda, Finite-size scaling analysis of the eigenstate thermalization hypothesis in a one-dimensional interacting Bose gas, Phys. Rev. E **87**, 012125 (2013).

[15] V. Alba, Eigenstate thermalization hypothesis and integrability in quantum spin chains, Phys. Rev. B **91**, 155123 (2015).

[16] S. Nandy, A. Sen, A. Das, and A. Dhar, Eigenstate Gibbs ensemble in integrable quantum systems, Phys. Rev. B **94**, 245131 (2016).

[17] J. M. Magán, Random Free Fermions: An Analytical Example of Eigenstate Thermalization, Phys. Rev. Lett. **116**, 030401 (2016).

[18] M. Haque and P. A. McClarty, Eigenstate thermalization scaling in majorana clusters: From chaotic to integrable Sachdev-Ye-Kitaev models, Phys. Rev. B **100**, 115122 (2019).

[19] M. Mierzejewski and L. Vidmar, Quantitative Impact of Integrals of Motion on the Eigenstate Thermalization Hypothesis, Phys. Rev. Lett. **124**, 040603 (2020).

[20] T. LeBlond, K. Mallayya, L. Vidmar, and M. Rigol, Entanglement and matrix elements of observables in interacting integrable systems, Phys. Rev. E **100**, 062134 (2019).

[21] M. Rigol, Breakdown of Thermalization in Finite One-Dimensional Systems, Phys. Rev. Lett. **103**, 100403 (2009).

[22] G. Biroli, C. Kollath, and A. M. Läuchli, Effect of Rare Fluctuations on the Thermalization of Isolated Quantum Systems, Phys. Rev. Lett. **105**, 250401 (2010).

[23] M. Rigol and L. F. Santos, Quantum chaos and thermalization in gapped systems, Phys. Rev. A **82**, 011604(R) (2010).

[24] L. F. Santos and M. Rigol, Localization and the effects of symmetries in the thermalization properties of one-dimensional quantum systems, Phys. Rev. E **82**, 031130 (2010).

[25] G. Roux, Finite-size effects in global quantum quenches: Examples from free bosons in an harmonic trap and the one-dimensional Bose-Hubbard model, Phys. Rev. A **81**, 053604 (2010).

[26] A. Motohashi, Thermalization of atom-molecule Bose gases in a double-well potential, Phys. Rev. A **84**, 063631 (2011).

[27] G. P. Brandino, A. De Luca, R. M. Konik, and G. Mussardo, Quench dynamics in randomly generated extended quantum models, Phys. Rev. B **85**, 214435 (2012).

[28] R. Steinigeweg, J. Herbrych, and P. Prelovšek, Eigenstate thermalization within isolated spin-chain systems, Phys. Rev. E **87**, 012118 (2013).

[29] H. Kim, T. N. Ikeda, and D. A. Huse, Testing whether all eigenstates obey the eigenstate thermalization hypothesis, Phys. Rev. E **90**, 052105 (2014).

[30] S. Sorg, L. Vidmar, L. Pollet, and F. Heidrich-Meisner, Relaxation and thermalization in the one-dimensional Bose-Hubbard model: A case study for the interaction quantum quench from the atomic limit, Phys. Rev. A **90**, 033606 (2014).

[31] R. Steinigeweg, A. Khodja, H. Niemeyer, C. Gogolin, and J. Gemmer, Pushing the Limits of the Eigenstate Thermalization Hypothesis Towards Mesoscopic Quantum Systems, Phys. Rev. Lett. **112**, 130403 (2014).

[32] K. R. Fratus and M. Srednicki, Eigenstate thermalization in systems with spontaneously broken symmetry, Phys. Rev. E **92**, 040103(R) (2015).

[33] R. Nandkishore and D. A. Huse, Many-body localization and thermalization in quantum statistical mechanics, Annu. Rev. Condens. Matter Phys. **6**, 15 (2015).

[34] A. Khodja, R. Steinigeweg, and J. Gemmer, Relevance of the eigenstate thermalization hypothesis for thermal relaxation, Phys. Rev. E **91**, 012120 (2015).

[35] R. Mondaini, K. R. Fratus, M. Srednicki, and M. Rigol, Eigenstate thermalization in the two-dimensional transverse field ising model, Phys. Rev. E **93**, 032104 (2016).

[36] A. Chandran, M. D. Schulz, and F. J. Burnell, The eigenstate thermalization hypothesis in constrained Hilbert spaces: A case study in non-Abelian anyo n chains, Phys. Rev. B **94**, 235122 (2016).

[37] D. J. Luitz and Y. Bar Lev, Anomalous Thermalization in Ergodic Systems, Phys. Rev. Lett. **117**, 170404 (2016).

[38] R. Mondaini and M. Rigol, Eigenstate thermalization in the two-dimensional transverse field ising model. II. Off-diagonal matrix elements of observables, Phys. Rev. E **96**, 012157 (2017).

[39] J. Sonner and M. Vielma, Eigenstate thermalization in the Sachdev-Ye-Kitaev model, J. High Energy Phys. 11 (2017) 149.

[40] Z. Lan and S. Powell, Eigenstate thermalization hypothesis in quantum dimer models, Phys. Rev. B **96**, 115140 (2017).

[41] T. Yoshizawa, E. Iyoda, and T. Sagawa, Numerical Large Deviation Analysis of the Eigenstate Thermalization Hypothesis, Phys. Rev. Lett. **120**, 200604 (2018).

[42] A. Dymarsky, N. Lashkari, and H. Liu, Subsystem eigenstate thermalization hypothesis, Phys. Rev. E **97**, 012140 (2018).

[43] N. Hunter-Jones, J. Liu, and Y. Zhou, On thermalization in the SYK and supersymmetric SYK models, J. High Energy Phys. 02 (2018) 142.
[44] D. Jansen, J. Stolpp, L. Vidmar, and F. Heidrich-Meisner, Eigenstate thermalization and quantum chaos in the Holstein polaron model, Phys. Rev. B **99**, 155130 (2019).
[45] I. M. Khaymovich, M. Haque, and P. A. McClarty, Eigenstate Thermalization, Random Matrix Theory, and Behemoths, Phys. Rev. Lett. **122**, 070601 (2019).
[46] C. Schönle, D. Jansen, F. Heidrich-Meisner, and L. Vidmar, Eigenstate thermalization hypothesis through the lens of autocorrelation functions, arXiv:2011.13958.
[47] R. Hamazaki and M. Ueda, Atypicality of Most Few-Body Observables, Phys. Rev. Lett. **120**, 080603 (2018).
[48] V. Khemani, C. R. Laumann, and A. Chandran, Signatures of integrability in the dynamics of rydberg-blockaded chains, Phys. Rev. B **99**, 161101(R) (2019).
[49] M. Brenes, T. LeBlond, J. Goold, and M. Rigol, Eigenstate Thermalization in a Locally Perturbed Integrable System, Phys. Rev. Lett. **125**, 070605 (2020).
[50] A. Polkovnikov, Quantum corrections to the dynamics of interacting bosons: Beyond the truncated Wigner approximation, Phys. Rev. A **68**, 053604 (2003).
[51] K. W. Mahmud, H. Perry, and W. P. Reinhardt, Quantum phase-space picture of Bose-Einstein condensates in a double well, Phys. Rev. A **71**, 023615 (2005).
[52] M. Hiller, T. Kottos, and T. Geisel, Complexity in parametric Bose-Hubbard Hamiltonians and structural analysis of eigenstates, Phys. Rev. A **73**, 061604(R) (2006).
[53] S. Mossmann and C. Jung, Semiclassical approach to Bose-Einstein condensates in a triple well potential, Phys. Rev. A **74**, 033601 (2006).
[54] E. M. Graefe and H. J. Korsch, Semiclassical quantization of an n-particle Bose-Hubbard model, Phys. Rev. A **76**, 032116 (2007).
[55] F. Trimborn, D. Witthaut, and H. J. Korsch, Beyond mean-field dynamics of small Bose-Hubbard systems based on the number-conserving phase-space approach, Phys. Rev. A **79**, 013608 (2009).
[56] A. Polkovnikov, Phase space representation of quantum dynamics, Ann. Phys. **325**, 1790 (2010).
[57] K. Pawłowski, P. Ziń, K. Rzażewski, and M. Trippenbach, Revivals in an attractive Bose-Einstein condensate in a double-well potential and their decoherence, Phys. Rev. A **83**, 033606 (2011).
[58] L. Simon and W. T. Strunz, Analytical results for Josephson dynamics of ultracold bosons, Phys. Rev. A **86**, 053625 (2012).
[59] L. Simon and W. T. Strunz, Time-dependent semiclassics for ultracold Bosons, Phys. Rev. A **89**, 052112 (2014).
[60] H. Veksler and S. Fishman, Semiclassical analysis of Bose-Hubbard dynamics, New J. Phys. **17**, 053030 (2015).
[61] T. Engl, J. D. Urbina, and K. Richter, Periodic mean-field solutions and the spectra of discrete Bosonic fields: Trace formula for Bose-Hubbard models, Phys. Rev. E **92**, 062907 (2015).
[62] T. Engl, J. D. Urbina, and K. Richter, The semiclassical propagator in Fock space: Dynamical echo and many-body interference, Philos. Trans. R. Soc. A **374**, 20150159 (2016).
[63] S. Ray, P. Ostmann, L. Simon, F. Grossmann, and W. T. Strunz, Dynamics of interacting bosons using the Herman-Kluk semiclassical initial value representation, J. Phys. A: Math. Theor. **49**, 165303 (2016).
[64] R. Dubertrand and S. Müller, Spectral statistics of chaotic many-body systems, New J. Phys. **18**, 033009 (2016).
[65] S. Tomsovic, P. Schlagheck, D. Ullmo, J.-D. Urbina, and K. Richter, Post-Ehrenfest many-body quantum interferences in ultracold atoms far out of equilibrium, Phys. Rev. A **97**, 061606(R) (2018).
[66] S. Tomsovic, Complex saddle trajectories for multidimensional quantum wave packet and coherent state propagation: Application to a many-body system, Phys. Rev. E **98**, 023301 (2018).
[67] J. Rammensee, J. D. Urbina, and K. Richter, Many-Body Quantum Interference and the Saturation of Out-of-Time-Order Correlators, Phys. Rev. Lett. **121**, 124101 (2018).
[68] R. A. Kidd, M. K. Olsen, and J. F. Corney, Quantum chaos in a Bose-Hubbard dimer with modulated tunneling, Phys. Rev. A **100**, 013625 (2019).
[69] P. Schlagheck, D. Ullmo, J. D. Urbina, K. Richter, and S. Tomsovic, Enhancement of Many-Body Quantum Interference in Chaotic Bosonic Systems: The Role of Symmetry and Dynamics, Phys. Rev. Lett. **123**, 215302 (2019).
[70] K. Nemoto, C. A. Holmes, G. J. Milburn, and W. J. Munro, Quantum dynamics of three coupled atomic Bose-Einstein condensates, Phys. Rev. A **63**, 013604 (2000).
[71] C. Weiss and N. Teichmann, Differences between Mean-Field Dynamics and n-Particle Quantum Dynamics as a Signature of Entanglement, Phys. Rev. Lett. **100**, 140408 (2008).
[72] T. F. Viscondi and K. Furuya, Dynamics of a Bose-Einstein condensate in a symmetric triple-well trap, J. Phys. A: Math. Theor. **44**, 175301 (2011).
[73] B. Gertjerenken and C. Weiss, Beyond-mean-field behavior of large Bose-Einstein condensates in double-well potentials, Phys. Rev. A **88**, 033608 (2013).
[74] A. R. Kolovsky, Bose-hubbard Hamiltonian: Quantum chaos approach, Int. J. Mod. Phys. B **30**, 1630009 (2016).
[75] C. Heinisch and M. Holthaus, Entropy production within a pulsed Bose-Einstein condensate, Z. Naturforsch. A **71**, 875 (2016).
[76] M. Rautenberg and M. Gärttner, Classical and quantum chaos in a three-mode Bosonic system, Phys. Rev. A **101**, 053604 (2020).
[77] M. Hiller, T. Kottos, and T. Geisel, Wave-packet dynamics in energy space of a chaotic trimeric Bose-Hubbard system, Phys. Rev. A **79**, 023621 (2009).
[78] G. Arwas, A. Vardi, and D. Cohen, Triangular Bose-Hubbard trimer as a minimal model for a superfluid circuit, Phys. Rev. A **89**, 013601 (2014).
[79] X. Han and B. Wu, Ehrenfest breakdown of the mean-field dynamics of Bose gases, Phys. Rev. A **93**, 023621 (2016).
[80] R. Bürkle and J. R. Anglin, Threshold coupling strength for equilibration between small systems, Phys. Rev. A **99**, 063617 (2019).
[81] A. A. Bychek, P. S. Muraev, D. N. Maksimov, E. N. Bulgakov, and A. R. Kolovsky, Chaotic and regular dynamics in the three-site Bose-Hubbard model, AIP Conf. Proc. **2241**, 020007 (2020).

[82] A. R Kolovsky and A Buchleitner, Quantum chaos in the Bose-Hubbard model, Europhys. Lett. **68**, 632 (2004).

[83] C. Kollath, G. Roux, G. Biroli, and A. M. Läuchli, Statistical properties of the spectrum of the extended Bose-Hubbard model, J. Stat. Mech. (2010) P08011.

[84] J. de la Cruz, S. Lerma-Hernández, and J. G. Hirsch, Quantum chaos in a system with high degree of symmetries, Phys. Rev. E **102**, 032208 (2020).

[85] L. Pausch, E. G. Carnio, A. Rodríguez, and A. Buchleitner, Chaos and ergodicity across the energy spectrum of interacting bosons, arXiv:2009.05295.

[86] W. Beugeling, A. Bäcker, R. Moessner, and M. Haque, Statistical properties of eigenstate amplitudes in complex quantum systems, Phys. Rev. E **98**, 022204 (2018).

[87] A. Bäcker, M. Haque, and I. M. Khaymovich, Multifractal dimensions for random matrices, chaotic quantum maps, and many-body systems, Phys. Rev. E **100**, 032117 (2019).

[88] D. J. Luitz, I. M. Khaymovich, and Y. B. Lev, Multifractality and its role in anomalous transport in the disordered XXZ spin-chain, SciPost Phys. Core **2**, 6 (2020).

[89] W. Beugeling, A. Andreanov, and M. Haque, Global characteristics of all eigenstates of local many-body Hamiltonians: Participation ratio and entanglement entropy, J. Stat. Mech. (2015) P02002.

[90] C. Liu, X. Chen, and L. Balents, Quantum entanglement of the Sachdev-Ye-Kitaev models, Phys. Rev. B **97**, 245126 (2018).

[91] M. Haque, P. A. McClarty, and I. M. Khaymovich, Entanglement of midspectrum eigenstates of chaotic many-body systems–deviation from random ensembles, arXiv:2008.12782.

[92] J. Gemmer, M. Michel, and G. Mahler, *Quantum Thermodynamics: Emergence of Thermodynamic Behavior Within Composite Quantum Systems*, Lecture Notes in Physics (Springer, Berlin, 2009).

[93] P. Reimann, Typicality for Generalized Microcanonical Ensembles, Phys. Rev. Lett. **99**, 160404 (2007).

[94] P. Reimann, Typicality of pure states randomly sampled according to the Gaussian adjusted projected measure, J. Stat. Phys. **132**, 921 (2008).

[95] S. Lloyd, Pure state quantum statistical mechanics and black holes, Ph.D. thesis, Rockefeller University, 1988.

[96] F. Alet and N. Laflorencie, Many-body localization: An introduction and selected topics, C. R. Phys. **19**, 498 (2018).

[97] C. J. Turner, A. A. Michailidis, D. A. Abanin, M. Serbyn, and Z. Papić, Weak ergodicity breaking from quantum many-body scars, Nat. Phys. **14**, 745 (2018).

[98] M. Feingold and A. Peres, Regular and chaotic motion of coupled rotators, Physica D **9**, 433 (1983).

[99] M. Feingold, N. Moiseyev, and A. Peres, Ergodicity and mixing in quantum theory. II, Phys. Rev. A **30**, 509 (1984).

[100] D. T. Robb and L. E. Reichl, Chaos in a two-spin system with applied magnetic field, Phys. Rev. E **57**, 2458 (1998).

[101] J. Emerson and L.E. Ballentine, Characteristics of quantum-classical correspondence for two interacting spins, Phys. Rev. A **63**, 052103 (2001).

[102] L. E. Ballentine, Quantum-to-classical limit in a Hamiltonian system, Phys. Rev. A **70**, 032111 (2004).

[103] Y. Fan, S. Gnutzmann, and Y. Liang, Quantum chaos for nonstandard symmetry classes in the Feingold-Peres model of coupled tops, Phys. Rev. E **96**, 062207 (2017).

[104] S. Pappalardi, A. Russomanno, B. Žunkovič, F. Iemini, A. Silva, and R. Fazio, Scrambling and entanglement spreading in long-range spin chains, Phys. Rev. B **98**, 134303 (2018).

[105] A. Piga, M. Lewenstein, and J. Q. Quach, Quantum chaos and entanglement in ergodic and nonergodic systems, Phys. Rev. E **99**, 032213 (2019).

[106] A. Lerose and S. Pappalardi, Bridging entanglement dynamics and chaos in semiclassical systems, Phys. Rev. A **102**, 032404 (2020).

[107] T. Xu, T. Scaffidi, and X. Cao, Does Scrambling Equal Chaos? Phys. Rev. Lett. **124**, 140602 (2020).

[108] S. Pappalardi, A. Polkovnikov, and A. Silva, Quantum echo dynamics in the Sherrington-Kirkpatrick model, SciPost Phys. **9**, 21 (2020).

[109] D. Mondal, S. Sinha, and S. Sinha, Chaos and quantum scars in a coupled top model, Phys. Rev. E **102**, 020101(R) (2020).

[110] M. A. Bastarrachea-Magnani, S. Lerma-Hernández, and J. G. Hirsch, Comparative quantum and semiclassical analysis of atom-field systems. II. Chaos and regularity, Phys. Rev. A **89**, 032102 (2014).

[111] M. A. Bastarrachea-Magnani, B. L. del Carpio, S. Lerma-Hernández, and J. G. Hirsch, Chaos in the Dicke model: Quantum and semiclassical analysis, Phys. Scr. **90**, 068015 (2015).

[112] S. Ray, A. Ghosh, and S. Sinha, Quantum signature of chaos and thermalization in the kicked Dicke model, Phys. Rev. E **94**, 032103 (2016).

[113] M. A. Bastarrachea-Magnani, B. López-del Carpio, J. Chávez-Carlos, S. Lerma-Hernández, and J. G. Hirsch, Delocalization and quantum chaos in atom-field systems, Phys. Rev. E **93**, 022215 (2016).

[114] R. J. Lewis-Swan, A. Safavi-Naini, J. J. Bollinger, and A. M. Rey, Unifying scrambling, thermalization and entanglement through measurement of fidelity out-of-time-order correlators in the Dicke model, Nat. Commun. **10**, 1581 (2019).

[115] J. Chávez-Carlos, B. López-del Carpio, M. A. Bastarrachea-Magnani, P. Stránský, S. Lerma-Hernández, L. F. Santos, and J. G. Hirsch, Quantum and Classical Lyapunov Exponents in Atom-Field Interaction Systems, Phys. Rev. Lett. **122**, 024101 (2019).

[116] Q. Wang and M. Robnik, Statistical properties of the localization measure of chaotic eigenstates in the Dicke model, Phys. Rev. E **102**, 032212 (2020).

[117] D. Villaseñor, S. Pilatowsky-Cameo, M. A. Bastarrachea-Magnani, S. Lerma-Hernández, L. F. Santos, and J. G. Hirsch, Quantum vs classical dynamics in a spin-Boson system: manifestations of spectral correlations and scarring, New J. Phys. **22**, 063036 (2020).

[118] S. Pilatowsky-Cameo, J. Chávez-Carlos, M. A. Bastarrachea-Magnani, P. Stránský, S. Lerma-Hernández, L. F. Santos, and J. G. Hirsch, Positive quantum Lyapunov exponents in

experimental systems with a regular classical limit, Phys. Rev. E **101**, 010202(R) (2020).

[119] S. Sinha and S. Sinha, Chaos and Quantum Scars in Bose-Josephson Junction Coupled to a Bosonic Mode, Phys. Rev. Lett. **125**, 134101 (2020).

[120] V. Oganesyan and D. A. Huse, Localization of interacting fermions at high temperature, Phys. Rev. B **75**, 155111 (2007).

[121] Y. Y. Atas, E. Bogomolny, O. Giraud, and G. Roux, Distribution of the Ratio of Consecutive Level Spacings in Random Matrix Ensembles, Phys. Rev. Lett. **110**, 084101 (2013).